THE SHEAR ALFVÉN CONTINUUM IN AN ASYMMETRIC MHD EQUILIBRIUM

A. Salat and J. A. Tataronis*

IPP III/219 July 1997

MAX-PLANCK-INSTITUT FÜR PLASMAPHYSIK

85748 GARCHING BEI MÜNCHEN

MAX-PLANCK-INSTITUT FÜR PLASMAPHYSIK

GARCHING BEI MÜNCHEN

THE SHEAR ALFVÉN CONTINUUM IN AN ASYMMETRIC MHD EQUILIBRIUM

A. SALAT AND J. A. TATARONIS*

IPP III/219 July 1997

* University of Wisconsin-Madison, 1500 Engineering DR, Madison, WI 53706, USA

Die nachstehende Arbeit wurde im Rahmen des Vertrages zwischen dem Max-Planck-Institut für Plasmaphysik und der Europäischen Atomgemeinschaft über die Zusammenarbeit auf dem Gebiete der Plasmaphysik durchgeführt.

Abstract

The Alfvén continuum in an asymmetric plasma configuration that is an exact solution of the equilibrium equations of ideal magnetohydrodynamics is treated. The equilibrium is parallel to an infinite straight magnetic axis about which the magnetic lines of force form closed magnetic surfaces. For small plasma beta, the Alfvén continuum is governed by an ordinary differential equation along the magnetic force lines. Properties of the equation are explored, and the Alfvén continuous spectrum is determined. It is found that the Alfvén continuum has two components: a localized component characterized by modes that decay to zero along magnetic field lines, and a non-localized component characterized by modes that approach non-zero constants at the plasma ends. The spectrum of the localized component is restricted to real frequencies; the spectrum of the non-localized component covers the entire complex frequency plane. For real and imaginary frequencies, a detailed study of the continuum is made. It is found that the non-localized modes can be joined generally with those on neighboring field lines to form modes that smoothly cover the entire magnetic surface. The localized modes, the *nonsymmetry induced Alfvén eigenmodes* (NAE), do not occur in symmetric plasmas.

1. Introduction

The shear Alfvén continuum of ideal magnetohydrodynamics (MHD) has received considerable interest and attention in the past because of its potential importance for plasma heating and current drive, and because of its possible effects on plasma stability. Applications of the shear Alfvén wave continuum modes are based on the spatial singularity that characterizes the mode amplitude. This singularity reflects the existence of a continuous spectrum of eigenmodes. What is known about the Alfvén continuum has arisen principally from studies of MHD wave phenomena in equilibria with spatial symmetries, such as the one-dimensional cylindrical screw pinch and the two-dimensional toroidal tokamak. The shear Alfvén continuum in asymmetric equilibria has received minimal attention. In the absence of spatial symmetry, existence of MHD equilibria has not been clearly established. This lack of an existence proof and the mathematical difficulties associated with asymmetric geometries have likely impeded studies of Alfvén wave behavior in three-dimensional plasmas. Recently, however, a class of asymmetric MHD equilibria, each of which is an exact solution of the ideal MHD equations, has been found.[1] These particular equilibria are parallel to a straight, infinite, magnetic axis. The magnetic lines of force twist about the axis and form closed magnetic surfaces. The study reported here treats the shear Alfvén continuum in this class of straight asymmetric MHD equilibria.[2] Emphasis is placed on small beta plasmas. Under the condition of small beta, an ordinary differential equation along the force lines of the equilibrium magnetic field governs the shear Alfvén continuum mode. In the vicinity of the magnetic axis, the mode equation can be expressed in an explicit form that can be solved analytically along particular magnetic field lines. The analytic solution reveals that the Alfvén continuum has two components: a localized component characterized by modes that decay to zero along magnetic field lines, and a non-localized component characterized by modes that approach non-zero constants at the plasma ends. The allowed frequencies of the localized modes are real and discrete, while the non-localized modes exist for all complex frequencies. Since the non-localized mode frequencies have no restrictions, instability is implied if the frequency has a negative imaginary part. This instability, however, depends on boundary conditions specified at the ends of the infinite plasma configuration. It is not excited by forces internal to the plasma. The localized modes, which in this study are termed

nonsymmetry induced Alfvén eigenmodes (NAE), are new. They do not occur in symmetric plasma configurations. Numerical solutions of the Alfvén continuum equation on other field lines and on magnetic surfaces further from the magnetic axis confirm the generality of this classification of the continuum modes. Properties of NAE will be described. Although this study is based on a particular asymmetric straight configuration, it is speculated that the results have relevance in asymmetric toroidal plasmas.

The plan of the paper is as follows. In Sect. 2, we present and discuss the equations that will serve as the basis of our spectral analysis. Section 3 introduces the particular three-dimensional equilibrium that we treat. In Sect. 4 we introduce the characteristic form of the Alfvén spectral equation and describe features of the localized and non-localized solutions of this equation. Section 5 deals with solutions of the characteristic spectral equation on magnetic field lines near the magnetic axis. In this Section, the NAE's are introduced. The spectrum on field lines that lie beyond the near region of the magnetic axis is treated in Sect. 6. We summarize the results of our analysis and the key conclusions in Sect. 7.

2. Basic Equations and Problem Formulation

Our spectral analysis is based on the linearized equations of ideal compressible MHD. We assume that the equilibrium state of the plasma is characterized by a magnetic field $\mathbf{B}$, the associated current density $\mathbf{J}$, and a pressure P. Force balance on a fluid element governs the equilibrium configuration,

$$\nabla P = \mathbf{J} \times \mathbf{B} \; . \tag{1}$$

A fundamental assumption of this study is that Eq. (1) is satisfied by a magnetic field that spans nested surfaces, $F(\mathbf{r}) \equiv$ const, with $\mathbf{B} \cdot \nabla F = 0$. In the presence of spatial symmetry, such solutions of Eq. (1) do exist. In the absence of spatial symmetry, existence of equilibrium solutions has been questionable.[3] Recently, however, a class of spatially asymmetric equilibria, each of which is an exact solution of Eq. (1), has been found.[1] These particular equilibria are parallel to a straight, infinite, magnetic axis. The magnetic lines of force twist about the axis and form closed magnetic surfaces. It is this class of MHD equilibria that is assumed here.

Wave propagation is governed by the linearized MHD equations,[4]

$$i\omega\mu_0\rho\mathbf{v} = (\mathbf{B}\cdot\nabla)\mathbf{b} + (\mathbf{b}\cdot\nabla)\mathbf{B} - \mu_0\nabla p^* \ , \tag{2}$$

$$i\omega\mathbf{b} = (\mathbf{B}\cdot\nabla)\mathbf{v} - (\mathbf{v}\cdot\nabla)\mathbf{B} - \mathbf{B}\nabla\cdot\mathbf{v} \ , \tag{3}$$

$$i\omega p = -\mathbf{v}\cdot\nabla P - \gamma P\nabla\cdot\mathbf{v} \ , \tag{4}$$

where $\mathbf{b}$, $\mathbf{v}$, and p represent, respectively, the magnetic field, the velocity field and the fluctuating pressure of the wave, p^* represents the total perturbed plasma pressure, $p^* \equiv p + \mathbf{B}\cdot\mathbf{b}/\mu_0$, and the parameters μ_0 and γ designate, respectively, the vacuum permeability and the ratio of specific heats. In addition, a harmonic time dependence of the form $\exp(i\omega t)$ with frequency ω has been assumed.

The derivation of the Alfvén continuum equations from Eqs. (2)-(4) for general three-dimensional MHD equilibria with magnetic surfaces has been given in Ref. 5. Alfvén waves are found to be coupled with slow magnetosonic waves, in general. In the limit of small plasma beta, $\beta \ll 1$, this coupling is removed, and a single scalar differential equation for the waves in the Alfvén continuum is obtained.[6] Our treatment is based on this equation, which is Eq. (9) in our manuscript. For the sake of completeness, we briefly summarize here the main steps of its derivation.[6] Our justification for taking cases with $P \to 0$ is that we want to focus our interest on the effects of nonsymmetric geometry and therefore want to eliminate distracting side effects.

It is convenient to introduce magnetic surface coordinates (r^1, r^2, r^3), where r^1 is identical to the magnetic surface function F, $r^1 \equiv F$, while r^2 and r^3 label points on the magnetic surfaces $r^1 \equiv$ const. Associated with this set of curvilinear coordinates are contravariant and covariant components of each vector field. Let v^i and b^i be the contravariant components of $\mathbf{v}$ and $\mathbf{b}$ associated with the coordinates r^i, i.e. $v^i \equiv \mathbf{v}\cdot\nabla r^i$, $i = 1, 2, 3$, etc. In the system of coupled differential equations for $(p^*, v^1, v^2, v^3, b^1, b^2, b^3)$ that results from Eqs. (2)-(4), only two equations contain normal derivatives out of the magnetic surfaces, namely

$$\frac{\partial p^*}{\partial r^1} = \gamma_1(v^1) + \gamma_2(p^*) + \gamma_3(b^3) \ , \tag{5}$$

$$\frac{\partial v^1}{\partial r^1} = \gamma_4(v^1) + \gamma_5(p^*) + \gamma_6(v^3) \ . \tag{6}$$

If both b^3 and v^3 in Eqs. (5) and (6) can be expressed in terms of p^* and v^1, the normal derivative of p^* and v^1 (and of the other components) exist and

are well behaved. The contravariant component b^3 can be expressed explicitly in terms of v^1, v^3 and p^*

$$b^3 = G(v^1, v^3, p^*) \ . \tag{7}$$

The elimination of v^3, however, causes problems. It can be expressed, ultimately, in terms of v_3, the covariant component of $\mathbf{v}$ associated with r^3, which in turn is governed by an inhomogeneous partial differential equation

$$\frac{B^2}{(\nabla F)^2}\mathbf{B}\cdot\nabla\left[\frac{(\nabla F)^2}{B^2}\mathbf{B}\cdot\nabla v_3\right] + \mu_0\rho\omega^2 v_3 = H(v^1, p^*) \ , \tag{8}$$

where B^2 and $(\nabla F)^2$ designate, respectively, $\mathbf{B}\cdot\mathbf{B}$ and $\nabla F\cdot\nabla F$. The symbols γ_1 to γ_6 in Eqs. (5) and (6), and G and H in Eqs. (7) and (8) denote functionals. They represent linear polynomials in their arguments, or in derivatives thereof, in directions tangential to the magnetic surfaces. Details are given in Ref. 6.

Equation (8) is a partial differential equation with derivatives on the left-hand side appearing only through the operator $\mathbf{B}\cdot\boldsymbol{\nabla}$. Therefore, it is a hyperbolic equation with the lines of force of $\boldsymbol{B}$ as the characteristic lines. Along the characteristics, it becomes an ordinary differential equation. The problem is to find solutions Eq. (8) that are single-valued over magnetic surfaces. Existence of such solutions depends on solutions of the associated homogeneous equation

$$\frac{B^2}{(\nabla F)^2}\mathbf{B}\cdot\nabla\left[\frac{(\nabla F)^2}{B^2}\mathbf{B}\cdot\nabla u\right] + \mu_0\rho\omega^2 u = 0 \ . \tag{9}$$

If the only solution of Eq. (9) is the trivial null solution, $u \equiv 0$, then Eq. (8) can be solved for v_3, and the system defined by Eqs. (5) and (6) can be integrated to give analytic solutions. If Eq. (9) possesses a nontrivial solution, however, the inverse of Eq. (8) does not exist. In this case *singular* solutions about the magnetic surface $F = \text{const}$ under consideration may exist. Existence of solutions of Eq. (9) depends on ω and F. That set of ω for which Eq. (9) is solvable on a magnetic surface defines the low-β Alfvén continuum of ideal MHD.

Equation (9) corresponds in a certain sense to Alfvén waves propagating along and confined to the immediate vicinity of a magnetic field line. The vector fields $\mathbf{b}$ and $\mathbf{v}$ are polarized *within* the magnetic surface.[5] This polarization is produced by singling out the coordinate $r^1 = F$ as the deciding coordinate for singularities, as appears in Eqs. (5) and (6).

Other choices of the direction of singularities than above are also possible. The resulting Alfvén waves have components *out of* the magnetic surfaces as well. The distinction between these two types of Alfvén modes and their separate contribution to the MHD spectrum was worked out from a principal point of view in Refs. 7 and 8. If the normal component of the polarization does not vanish, the waves experience the full force of normal equilibrium gradients, such as the pressure gradient, the shear, etc. Consequently, this other type of Alfvén mode may easily become unstable under unfavorable conditions. Their contribution to the MHD spectrum, therefore, is called the "ballooning spectrum" in Ref. 8, in contrast to the "Alfvén continuum" part which is the subject of our investigation. In recent years also the stable part of the ballooning spectrum has gained widespread attention, since it comprises the "toroidicity induced Alfvén eigenmodes" (TAE) and their relatives. These modes are relevant e.g. in the context of scattering and ensuing loss of fast fusion alpha particles (see, e.g. Ref. 9 for two seminal papers on the subject). We do not discuss here this type of mode with normal component of polarization.

In the following Sections of this paper, the solvability of Eq. (9) for the asymmetric equilibrium found by Kaiser and Salat[1] is treated.

3. Equilibria without Continuous Symmetries

In Refs. 1 and 10, several classes of explicit MHD equilibria without continuous symmetries were derived. These asymmetric equilibria satisfy exactly Eq. (1). One such equilibrium that is particularly attractive for investigating linear wave propagation in low-β plasmas has the following magnetic field expressed in terms of (x, y, z) Cartesian coordinates,[1]

$$\mathbf{B} = \nabla \times [H(x,y,z)\nabla z] + \nabla \times \nabla \times [K(x,y,z)\nabla z] \,, \tag{10}$$

where

$$H(x,y,z) = \frac{h\eta}{\kappa}\left[\mathrm{e}^{\kappa z}\cos(\lambda x) + \mathrm{e}^{-\kappa z}\cos(\lambda y)\right] \,, \tag{11}$$

$$K(x,y,z) = \frac{k}{\lambda\kappa}\left[\mathrm{e}^{\kappa z}\cos(\lambda x) + \mathrm{e}^{-\kappa z}\cos(\lambda y)\right] \,, \tag{12}$$

$$\eta = \frac{\sqrt{\kappa^2 - \lambda^2}}{\kappa} \,. \tag{13}$$

The real constants h, k, and η in Eqs. (10)-(13) govern the strength of the magnetic field, while λ and κ are real constants that govern the spatial scale

lengths of the equilibrium configuration. Without any loss of generality, we assume that λ and κ are positive. The associated pressure of the configuration $P(x,y,z)$ is given by

$$P(x,y,z) = P_0 - 0.5(h^2+k^2)\eta^2 \left[e^{2\kappa z}\sin^2(\lambda x) + 2\left[1-\cos(\lambda x)\cos(\lambda y)\right] + e^{-2\kappa z}\sin^2(\lambda y)\right] . \tag{14}$$

Surfaces of constant pressure, $P(x,y,z) = \text{const}$, which are the magnetic surfaces spanned by Eq. (10), form a periodic distribution of closed nested surfaces about magnetic axes that are parallel to the z-axis from $z=-\infty$ to $z=+\infty$. The x and y coordinates of the magnetic axes are respectively $x = 2\pi m/\lambda$ and $y = 2\pi n/\lambda$, where m and n are integers. The pressure on each magnetic axis equals the constant P_0. Our spectral analysis will be based on the equilibrium configuration that is contained within the domain $-\pi/\lambda < x < \pi/\lambda$ and $-\pi/\lambda < y < \pi/\lambda$, with the z-axis of the Cartesian coordinate system as the magnetic axis.

In Eqs. (10) and (14), the limit $\lambda = \kappa$ is a constant pressure configuration with a curl-free and therefore a vacuum magnetic field. Although the pressure does not vary in space in this special case, nested magnetic surfaces still exist. They are defined by $\mathbf{B}\cdot\nabla F = 0$ where

$$F(x,y,z) \equiv e^{2\kappa z}\sin^2(\lambda x) + 2\left[1-\cos(\lambda x)\cos(\lambda y)\right] + e^{-2\kappa z}\sin^2(\lambda y) . \tag{15}$$

Surfaces of constant $F(x,y,z)$ are magnetic surface for $\eta = 0$, as well as for $\eta \neq 0$, because Eq. (14) can be cast in the form

$$\frac{P(x,y,z)-P_0}{\eta^2} = \frac{1}{2}(h^2+k^2)F(x,y,z) . \tag{16}$$

Since the right-hand side of Eq. (16) is independent of η, constant pressure and magnetic surfaces are defined by $F(x,y,z) = \text{const}$. The Cartesian components of the vacuum magnetic field that span constant $F(x,y,z)$ vacuum surfaces are derived by setting $\kappa = \lambda$ and $\eta = 0$ in Eqs. (10)-(12). They are given by

$$\begin{aligned} B_x &= -\frac{B_0}{2} e^{\kappa z}\sin(\kappa x) , \\ B_y &= \frac{B_0}{2} e^{-\kappa z}\sin(\kappa y) , \\ B_z &= \frac{B_0}{2}\left[e^{\kappa z}\cos(\kappa x) + e^{-\kappa z}\cos(\kappa y)\right] , \end{aligned} \tag{17}$$

where B_0 equals the value of B_z on the magnetic axis in the plane $z = 0$, which corresponds to $k = B_0/2$.

General geometrical features of the vacuum surfaces are illustrated in Fig. 1 for $F(x, y, z) = 1$ and the axial extent in the range $-2.3 < z < 2.3$. Bold lines identify four specific magnetic field lines: one in a "polar" position, one in an "equatorial" position, and two in intermediate positions. It can be seen that the transverse cross sections of the magnetic surfaces become progressively compressed and narrower towards the ends of the configuration. In the limit $z \to \pm\infty$, the cross section actually condenses into an infinitely thin sheet. As we will demonstrate later in this paper, part of the shear Alfvén wave spectrum is strongly influenced by this singularity. Further details of the magnetic surfaces $F = \text{const}$ are discussed in Ref. 1.

In the following Sections, the vacuum configuration $F(x, y, z) = \text{const}$ with $\lambda = \kappa$ will be used in conjunction with Eq. (9) to explore the shear Alfvén continuum in a low-β asymmetric MHD plasma. Explicit representations of the spatially dependent coefficients of the continuum partial differential equation will be readily derivable with Eqs. (15) and (17).

4. Alfvén Continuum of a Low-β Plasma

The Alfvén continuous spectrum of a low-β plasma is governed by Eq. (9). In this Section, we explore solutions of this equation for the asymmetric equilibrium defined by Eqs. (15) and (17).

Equation (9) is a second order hyperbolic partial differential equation. Along the characteristic lines, which are the force lines of $\mathbf{B}(\mathbf{r})$, the operator $\mathbf{B} \cdot \nabla$ becomes the directional derivative $B\,\mathrm{d}/\mathrm{d}\ell$, where ℓ is the arc length of the magnetic field line. The characteristic form of the Alfvén continuum equation is thus the ordinary differential equation,

$$\frac{\mathrm{d}}{\mathrm{d}\ell}\left[\frac{(\nabla F)^2}{B}\frac{\mathrm{d}u}{\mathrm{d}\ell}\right] + \frac{\mu_0(\nabla F)^2\rho\omega^2}{B^3}u = 0\,, \tag{18}$$

where the spatially dependent coefficients must be viewed as functions of ℓ because the position vector $\mathbf{r}$ depends on the path length along characteristic lines. Since the field lines extend from $z = -\infty$ to $z = +\infty$, it is advantageous to transform the independent variable to z from ℓ. Along a field line, we then regard the transverse coordinates x and y as functions z, where $x(z)$ and $y(z)$

are governed by

$$\frac{\mathrm{d}x}{\mathrm{d}z} = \frac{B_x}{B_z} \quad \text{and} \quad \frac{\mathrm{d}y}{\mathrm{d}z} = \frac{B_y}{B_z} \,. \tag{19}$$

The derivative $\mathrm{d}/\mathrm{d}\ell$ transforms as

$$\frac{\mathrm{d}}{\mathrm{d}\ell} = \frac{B_z}{B}\frac{\mathrm{d}}{\mathrm{d}z} \,. \tag{20}$$

Substituting Eq. (20) in Eq. (18) results in an ordinary differential equation that governs the z-dependence of u along a force line of $\mathbf{B}$,

$$\frac{\mathrm{d}}{\mathrm{d}z}\left[p(z)\frac{\mathrm{d}u}{\mathrm{d}z}\right] + \Lambda s(z)u(z) = 0 \,, \tag{21}$$

where

$$p = \frac{\hat{B}_z}{Q} \,, \qquad s = \frac{4}{\hat{B}_z Q} \,, \tag{22}$$

$$Q = \frac{\hat{B}^2}{(\nabla F)^2} \,, \tag{23}$$

and the parameter Λ equals the frequency squared divided by the square of the Alfvén speed on the magnetic axis,

$$\Lambda = \frac{\mu_0 \rho \omega^2}{B_0^2} \,. \tag{24}$$

The vector field $\hat{\mathbf{B}}$ that appears in in Eqs. (22) and (23) is the equilibrium magnetic field normalized with respect to $B_0/2$, $\hat{\mathbf{B}} \equiv 2\mathbf{B}/B_0$. The coefficients $p(z)$ and $s(z)$ depend on the solutions of Eq. (19) for $x(z)$ and $y(z)$. These equations can be solved explicitly up to quadratures, as demonstrated in Appendix A. Moreover, in some cases, they can be solved analytically, as we show in Sects. 5a and 5b. However, although quadratures do exist, they are not convenient to use. Numerical solutions of Eqs. (19) will in many cases be useful to specify $p(z)$ and $s(z)$.

Equation (21) governs the modes in the Alfvén continuum. The property of these modes, and therefore the nature of the Alfvén continuum, depends on the asymptotic behavior of $u(z)$ as $z \to \pm\infty$. Two general classes of solutions and therefore spectral components can be identified according to whether the integral $\int_{-\infty}^{+\infty} u^2(z)\,\mathrm{d}z$ is bounded or unbounded. If $\int_{-\infty}^{+\infty} u^2(z)\,\mathrm{d}z$ is bounded, Λ is a *discrete eigenvalue* and therefore in the *discrete spectrum*. The associated mode function $u(z)$ is a *discrete* or *localized eigenfunction*. If $\int_{-\infty}^{+\infty} u^2(z)\,\mathrm{d}z$

is unbounded, Λ is a *continuum eigenvalue* and therefore in the *continuous spectrum.* The associated mode function $u(z)$ in this case is a *continuum* or an *non-localized eigenfunction.* Another descriptive designation of the non-localized eigenfunctions that we shall employ is *extended eigenfunctions.* It is mentioned that "discrete" and "continuous" eigenfunctions refers to properties of the modes in the direction *parallel* to the magnetic field lines. Both modes belong to subsets within the set of modes of the *Alfvén continuum*, which is related to possible spatial singularities in the direction *normal* to magnetic surfaces.

The solution of Eq. (21) as an eigenvalue problem for Λ generally has to be approached numerically. However, analytical solutions can be found along certain field lines near the magnetic axis, which is the z-axis of the Cartesian coordinate system. In this special case, the field line equations given by Eq. (19) can be solved analytically, and this results in analytical expressions for the coefficients $p(z)$ and $s(z)$. On particular field lines even the eigenfunctions and eigenvalues can be derived analytically. This greatly facilitates the interpretation of the numerical results in the other cases. In Sect. 5 this near-axis case will be considered, while the general case will be addressed thereafter.

5. Alfvén Continuum near the Magnetic Axis

On magnetic surfaces close to the magnetic axis, the transverse coordinates satisfy the inequalities $|\kappa x| \ll 1$ and $|\kappa y| \ll 1$. In this Section, we explore the Alfvén continuum modes and the associated spectrum in this spatial region.

If $|\kappa x|$ and $|\kappa y|$ are sufficiently small, it is convenient to expand the Cartesian components of the magnetic field and the surface function F in Taylor series about the z-axis. To lowest order, Eqs. (17) and (15) yield, respectively,

$$\begin{aligned} \hat{B}_x &= -\,\mathrm{e}^{\kappa z}\kappa x\ , \\ \hat{B}_y &= \mathrm{e}^{-\kappa z}\kappa y\ , \\ \hat{B}_z &= \mathrm{e}^{\kappa z} + \mathrm{e}^{-\kappa z} \end{aligned} \tag{25}$$

and

$$F(x,y,z) = \left(\mathrm{e}^{\kappa z} + \mathrm{e}^{-\kappa z}\right)\left(\mathrm{e}^{\kappa z}x^2 + \mathrm{e}^{-\kappa z}y^2\right)\ . \tag{26}$$

These expressions in turn yield

$$\hat{B}^2 = \left(e^{\kappa z} + e^{-\kappa z}\right)^2 , \tag{27}$$

$$(\nabla F)^2 = 4\left(e^{\kappa z} + e^{-\kappa z}\right)^2 \left(e^{2\kappa z}x^2 + e^{-2\kappa z}y^2\right) . \tag{28}$$

With these approximate expressions for $\hat{B}^2$ and $(\nabla F)^2$, the following expressions for $p(z)$ and $s(z)$ are readily derived from Eqs. (21)-(23),

$$\begin{aligned} p(z) &= 4\left(e^{\kappa z} + e^{-\kappa z}\right)\left[e^{2\kappa z}x^2(z) + e^{-2\kappa z}y^2(z)\right] , \\ s(z) &= 16\,\frac{e^{2\kappa z}x^2(z) + e^{-2\kappa z}y^2(z)}{e^{\kappa z} + e^{-\kappa z}} , \end{aligned} \tag{29}$$

where $x(z)$ and $y(z)$ are the transverse coordinates of a magnetic field line that Eq. (19) defines. Using Eq. (25) for $B_x \equiv B_0\hat{B}_x/2$ and $B_y \equiv B_0\hat{B}_y/2$, Eq. (19) can be readily integrated. Solutions for $x(z)$ and $y(z)$ read

$$\begin{aligned} x(z) &= x_0\left(\frac{2e^{-\kappa z}}{e^{\kappa z} + e^{-\kappa z}}\right)^{1/2} , \\ y(z) &= y_0\left(\frac{2e^{\kappa z}}{e^{\kappa z} + e^{-\kappa z}}\right)^{1/2} , \end{aligned} \tag{30}$$

where x_0 and y_0 are the transverse coordinates of the field line in the plane $z = 0$. These expressions can also be derived using Eq. (A.5) of Appendix A. It should be noted that the functional forms of $x(z)$ and $y(z)$ are independent of the values F that label magnetic surfaces. This is not a general feature of the magnetic configuration. Only on surfaces close to the magnetic axis do $x(z)$ and $y(z)$ become independent of the value of F. This implies that the field lines near the magnetic axis have no shear. Equations (30) show that field lines with $x_0 = 0$ have $x(z) = 0$ for all z, and therefore remain in the "polar" plane defined by $x = 0$. Similarly, field lines with $y_0 = 0$ have $y(z) = 0$ for all z, and therefore remain in the "equatorial" plane defined by $y = 0$. This property of the field lines is a consequence of the mirror symmetry in x and y of the magnetic configuration. For all other field lines the slope $\mathrm{d}y/\mathrm{d}z$ is always positive for $y > 0$ and negative for $y < 0$. Therefore, in the direction of increasing z, the field lines depart from the equatorial plane into the north or south polar direction. Asymptotically, for $z \to +\infty$, for example, all field lines tend to a finite value of y, namely $y_\infty(y_0) = \sqrt{2}y_0$, and to $x_\infty = 0$. At the opposite end, the roles of x and y are interchanged. Typical magnetic field

lines that illustrate these properties are shown on the magnetic surfaces given by Fig. 1.

After substituting Eqs. (30) into Eqs. (29) and the resulting expressions for $p(z)$ and $s(z)$ into Eq. (21), the governing equation of the Alfvén continuum becomes

$$\frac{\cosh^2(\kappa z)}{e^{\kappa z}x_0^2 + e^{-\kappa z}y_0^2}\frac{d}{dz}\left[\left(e^{\kappa z}x_0^2 + e^{-\kappa z}y_0^2\right)\frac{du}{dz}\right] + \Lambda u = 0 . \tag{31}$$

The form of Eq. (31) can be simplified by transfoming the independent variable from z to a new variable τ that is defined by

$$\frac{dz}{d\tau} = \cosh(\kappa z) . \tag{32}$$

Substitution of Eq. (32) in Eq. (31) results in the following equation for $u(\tau)$,

$$\frac{d^2u}{d\tau^2} + \kappa\frac{x_0^2 - y_0^2}{e^{\kappa z}x_0^2 + e^{-\kappa z}y_0^2}\frac{du}{d\tau} + \Lambda u = 0 . \tag{33}$$

The integral of Eq. (32) that satisfies $\tau(0) = 0$ is

$$\tan(\kappa\tau) = \sinh(\kappa z) . \tag{34}$$

This expression implies that the infinite range of z, $-\infty < z < \infty$, transforms to a bounded range in τ, $-\pi/(2\kappa) < \tau < \pi/(2\kappa)$. Equation (34) further yields that $\tau(z) \to \pm\pi/(2\kappa)$ exponentially in $|z|$ as $z \to \pm\infty$,

$$\lim_{z\to\infty}\tau(z) = \frac{\pi}{2\kappa} - 2e^{-\kappa z}, \tag{35}$$

$$\lim_{z\to-\infty}\tau(z) = -\frac{\pi}{2\kappa} + 2e^{\kappa z}. \tag{36}$$

Because the range of τ over the plasma configuration is bounded, the identification of the spectrum that Eq. (33) governs is considerably simplified. The spectrum is dependent on the behavior of $u(\tau)$ as $\tau \to \pm\pi/(2\kappa)$, which corresponds to $z \to \pm\infty$. If x_0 and y_0 are not zero, the coefficient of $du/d\tau$ in Eq. (33) approaches zero in both limits. Therefore, assuming that $du/d\tau$ is bounded and that x_0 and y_0 are not zero, the limiting spectral equation as $\tau \to \pm\pi/(2\kappa)$ is

$$\frac{d^2u}{d\tau^2} + \Lambda u = 0 . \tag{37}$$

The two special cases $x_0 = 0$ and $y_0 = 0$ will be taken up in Sect. 5b. Equation (37) is a second order ordinary differential equation with constant coefficients.

Therefore, it is readily solved analytically. For $\Lambda \neq 0$, the general solution can be expressed as

$$u(\tau) = C_1 e^{i\sqrt{\Lambda}\tau} + C_2 e^{-i\sqrt{\Lambda}\tau} \ , \tag{38}$$

where C_1 and C_2 are arbitrary integration constants. Because $\tau(z)$ is bound for all z, the implication of Eq. (33) is that for all values of Λ and therefore for all values of the frequency ω, the solutions of Eq. (33) asymptotically tend toward constants, which means that $u(z)$ is bounded over the infinite range $-\infty < z < \infty$ for any complex ω. The implication of this key result is that the entire complex ω-plane belongs to the continuous spectrum. Continuous spectra of this type have previously been identified and described.[11] For particular combinations of the integration constants, $u(z)$ may actually vanish in the limit $z \to \infty$. If it can be established that $u(z)$ also vanishes as $z \to -\infty$, the associated value of ω would belong to the discrete component of the spectrum. In order to establish existence of a discrete spectrum, it is necessary to integrate Eq. (33) over the infinite range $-\infty < z < \infty$.

It is pointed out that for $\Lambda = 0$ Eq. (37) has a nontrivial solution that is linear in τ. Because τ is bounded, this special solution also belongs to the continuous component of the spectrum.

5a. Magnetic Field Lines $x_0^2 = y_0^2$

One particular case of Eq. (33) that can be treated analytically is $x_0^2 = y_0^2$. This case governs the Alfvén spectrum along the four magnetic field lines that lie in the middle of the quadrants of the $z = 0$ plane on a fixed magnetic surface. With $x_0^2 = y_0^2$, Eq. (33) becomes identically Eq. (37). Therefore, the general solution for $u(\tau)$ for all τ in the range $-\pi/(2\kappa) < \tau < \pi/(2\kappa)$ is Eq. (38). As already pointed out, the entire complex ω plane belongs to the continuous spectrum. In addition to the continuous spectrum, there is also a discrete spectrum. Discrete modes require $u(z) \to 0$ as $z \to \pm\infty$. By choosing the integration constants C_1 and C_2 appropriately in Eq. (38), it is readily established that the modes in the discrete spectrum are given by

$$\begin{aligned} u_m(z) &= \cos[m \arctan(\sinh z)] \ , \quad \text{for } m = 1,\ 3,\ 5, \ldots \ , \\ u_m(z) &= \sin[m \arctan(\sinh z)] \ , \quad \text{for } m = 2,\ 4,\ 6, \ldots \end{aligned} \tag{39}$$

where to simplify the notation the free integration constant and the parameter κ have been set equal to unity. To return κ explicitly into the expressions

for $u(z)$, only two replacements are required: Λ/κ^2 in place of Λ and κz in place of z. Thus, no loss of generality is incurred by assuming $\kappa = 1$ from the outset. This will be done in the analysis that follows. The discrete eigenvalues associated with each value of the integer m read

$$\Lambda_m = m^2 \ . \tag{40}$$

This shows that the frequencies in the discrete spectrum are real, and that the associated plasma motion is stable. With the help of trigonometric identities, the expressions for the eigenmodes can be expressed in other forms. For example, the lowest three eigenmodes modes can be expressed as

$$\begin{aligned} u_1(z) &= \frac{1}{\cosh z} \ , \\ u_2(z) &= \frac{\sinh z}{\cosh^2 z} \ , \\ u_3(z) &= \frac{1 - 3\sinh^2 z}{\cosh^3 z} \ . \end{aligned} \tag{41}$$

In Fig. 2, the eigenfunctions $u_1(z)$ and $u_{10}(z)$, with eigenvalues $\Lambda_1 = 1$ and $\Lambda_{10} = 100$, respectively, are shown. The mode $u_1(z)$, which is the simplest one computationally, will be used repeatedly for comparison with other cases.

It is pointed out that the occurrence of modes in the Alfvén continuum that are localized on magnetic field lines, i.e. that have a finite longitudinal extension along a field line, is an effect not reported previously. Localized modes on magnetic field lines result from the lack of a continuous symmetry in the configuration. In axial symmetry, for example, whatever the details, the coefficients of the eigenmode equation are periodic functions of the poloidal angle alone. In this case all solutions are known qualitatively from the Floquet theory of differential equations with periodic coefficients.[12] Of course, none of the solutions is localized.

Discrete Alfvén modes in a nonaxisymmetric toroidal (nonequilibrium) configuration, in contrast to a straight configuration, were discussed and investigated numerically in Ref. 13. A similarity between the Alfvén eigenmode equation in nonsymmetric toroidal geometry and the Schrödinger equation with quasiperiodic coefficients was observed. For the latter equation the existence of localized modes, in addition to extended modes, is known.[14] The configuration treated in Ref. 13, however, was not an MHD equilibrium but a

simplistic δ-function-type model. In this configuration a transition of a particular extended surface-covering mode into a localized mode on a field line was observed if the torus was made progressively fatter. A transition from continuum Alfvén modes to localized Alfvén modes was obtained also in a simplistic model of force free equilibria if the magnetic field lines are sufficiently chaotic.[15]

It may be instructive to compare the occurrence of discrete modes here and in the "ballooning spectrum", mentioned in Sec. 2. In the Alfvén continuum the axisymmetry of the coefficients in the mode equation can be broken only by the nonsymmetry of the equilibrium itself. In the "ballooning spectrum" discrete TAE modes are found already in axisymmetric configurations.[9] In the latter case finite shear separates neighboring field lines on different magnetic surfaces in a secular way. This also breaks the axisymmetry in the mode equation.

Continuum modes for the $x_0^2 = y_0^2$ case are represented by Eq. (38) with no constraint placed on Λ. By choosing the integration constants C_1 and C_2 appropriately, symmetric and antisymmetric mode $u_s(z)$ and $u_a(z)$, respectively, result,

$$u_s(z) = \cos\left[\sqrt{\Lambda}\arctan(\sinh z)\right] , \tag{42}$$

$$u_a(z) = \sin\left[\sqrt{\Lambda}\arctan(\sinh z)\right] . \tag{43}$$

As $z \to \pm\infty$, both modes approach non-zero contants. Figure 3 illustrates the spatial features of these modes for Λ real and positive. For the symmetric mode, Λ is set equal to $1/\sqrt{3}$; for the antisymmtric mode, Λ is set equal to $100/\sqrt{3}$.

An important issue related to the continuum modes is stability. Since no restriction is placed on the frequency, complex ω with negative imaginary part is allowed. Such modes are unstable. The mathematical reason why ω may be complex is the finite range of the independent variable τ in Eqs. (33) and (38). Since τ cannot exceed $\pi/(2\kappa)$ nor be less than $-\pi/(2\kappa)$, $u(z)$ in Eq. (38) is bounded in magnitude for any complex ω and therefore Λ. Only if $\kappa = 0$ can $|u(z)|$ be unbounded. Another way to identify possible restrictions on ω is to derive from Eq. (33) a bilinear functional representation of Λ. If Eq. (21) is multiplied by the complex conjugate of $u(z)$ and then integrated from $z = -\infty$ to $z = +\infty$, one obtains after partial integration

$$\Lambda \int_{-a}^{+a} s|u|^2 \, \mathrm{d}z = R + \int_{-a}^{+a} p \left|\frac{\mathrm{d}u}{\mathrm{d}z}\right|^2 \mathrm{d}z , \tag{44}$$

where

$$R(u^*, u) \equiv -pu^* \frac{\mathrm{d}u}{\mathrm{d}z}\bigg|_{-a}^{+a}, \tag{45}$$

and a approaches infinity. Periodicity of the configuration together with periodicity of the modes with respect to z would imply $R(u^*, u) = 0$. Under these conditions, and since both p and s are positive for all z, Eq. (44) would imply that Λ is real and greater than or equal to zero, and therefore a stable continuum. Our configuration, however, is not periodic in z, as readily established with Eq. (17) and Fig. 1, and therefore $R(u^*, u)$ is not manifestly zero. Consequently, Eq. (44) alone cannot imply stability of the continuum. Under certain conditions, $R(u^*, u)$ can actually be simultaneously negative and larger in magnitude than the integral in the right-hand side of (44). This suggests that an unstable continuum is in fact feasible.

A factor that plays a pivotal role regarding the existence of the unstable continuum is the singular end-regions of the magnetic configuration, $z \to \pm\infty$. Both regions are characterized by $B \to \infty$. Because B attains infinity, the Fourier mode amplitude $u(z)$ attains a constant bounded value at each end of the configuration for any complex ω. This implies that the associated time-harmonic Fourier mode $u(z, t)$ could be specified at $z = \pm\infty$. For example, it is possible to assume

$$\lim_{z \to -\infty} u(z, t) \to \mathrm{e}^{i\omega t} . \tag{46}$$

For finite z, the functional form of the Fourier mode is found by multiplying Eq. (38) by $\exp(i\omega t)$ and setting $C_1 = \exp[i\pi/(2c_A)]$ and $C_2 = 0$,

$$u(z, t) = \exp i\omega \left[t - \frac{1}{c_A}\tau(z) - \frac{\pi}{2c_A} \right] , \tag{47}$$

where Λ has been expressed as, $\Lambda \equiv \omega^2/c_A^2$. Here, c_A is the Alfvén speed on the magnetic axis in the plane $z = 0$, $c_A \equiv B_0/\sqrt{\mu_0 \rho}$. Equation (47) represents a wave that propagates towards $z = \infty$. If the imaginary part $\Im(\omega) < 0$, the magnitude of the wave amplitude $|u(z, t)|$ increases exponentially with increasing t for any z. The unstable continuum modes are of this type. This "continuum instability", however, should not be viewed as one driven by forces internal to the plasma since its existence is tied to appropriate data that must be specified at the end regions of the plasma configuration. It is mentioned that the stable and unstable continuum modes can be interpreted in terms of waves propagating along magnetic field lines. A treatment of the governing

wave equation and the initial value problem related to the unstable continuum will be reported in a separate publication.

Within the context of unstable modes, it is appropriate to discuss the conditions under which Λ, which is proportional to ω^2, would be real. Modes from the Alfvén continuum form a subclass of MHD modes. For MHD modes in general, it is well known that for configurations of finite extent and for suitable boundary conditions on the plasma surface, the mode equations are self-adjoint and consequently ω^2 is real.[16] The same conclusion would hold for periodic boundary conditions. When the configuration is straight and open, as is the one that we are currently exploring, these premises do not hold. However, in order to relate our results to a torus, which requires periodic boundary conditions, it is reasonable to assume self-adjointness and hence reality of Λ. In appendix B the boundary conditions compatible with self-adjointness of our mode equation, Eq. (31), are explored. The numerical solutions that we present below are based on real Λ.

Examples of unstable continuum modes are shown in Fig. 4 for two symmetric cases. It is evident that the modes are stronger in the end regions than in the central regions. At a larger value of $|\Lambda|$ (solid curve with $\Lambda = -100/\sqrt{3}$), this effect is more pronounced than at Λ close to the marginal point (dashed curve with $\Lambda = -1/\sqrt{3}$). It can easily be seen analytically that unstable continuum modes can at most have one zero crossing. Antisymmetric versions, therefore, qualitatively look like their symmetric counterparts, except that at $z = 0$ they continue with $u(z) = -u(-z)$.

It is instructive to comment at this point on the Alfvén spectrum in the limit $\kappa = 0$. In this case, the magnetic field goes over into a constant straight B_z field. Equation (31), the spectral equation, simply becomes $\mathrm{d}^2u/\mathrm{d}z^2 + \Lambda u = 0$, which has the general solution $u(z) = C_1 \exp(i\sqrt{\Lambda}z) + C_2 \exp(-i\sqrt{\Lambda}z)$. This result implies propagation at the familiar Alfvén phase speed $\omega/k_z = B_0/\sqrt{\mu_0\rho}$. Complex wave frequency in this case would imply spatial growth of the wave amplitude. Consequently, the wave frequency ω must be real, implying that $\Lambda > 0$. Moreover, all real ω belong to the continuous spectrum since the integral $\int_{-\infty}^{+\infty} u^2(z)\,\mathrm{d}z$ diverges. There are no discrete modes. As we have demonstrated, the effect of the three-dimensionality and of the singular end regions in the case $\kappa \neq 0$ is that some values of Λ are transferred from the continuum into the newly created discrete spectrum, and that the oscillations of the extended modes are suppressed in favor of a nonzero constant value of

$u(z)$, in the end regions.

So far, from the analytic solvability of Eqs. (31), (33), a fairly complete overview of the spectrum on the "central" field lines with $x_0^2 = y_0^2$ was obtained. It turns out that Eq. (33) can be solved analytically also on the special "limiting" field lines at $y_0 \equiv 0$ ("equatorial" lines) or $x_0 \equiv 0$ ("polar" lines). The cases $y_0 = 0$ and $x_0 = 0$ are treated in the following Section. Since at one end of the configuration such field lines run along a thin ridge and on the other end in the middle of a flat region, a pronounced asymmetry between $z \to +\infty$ and $z \to -\infty$ is to be expected for the eigenfunctions.

5b. Magnetic Field Lines $y_0 = 0$ and $x_0 = 0$

For the special field line $y_0 = 0$, it is best to base the spectrum analysis on Eq. (31). With y_0 set equal to zero, it reduces to

$$\frac{\cosh^2 z}{\mathrm{e}^z} \frac{\mathrm{d}}{\mathrm{d}z}\left[\mathrm{e}^z \frac{\mathrm{d}u}{\mathrm{d}z}\right] + \Lambda u = 0 \,, \tag{48}$$

where κ has been set equal to unity. Transformations of the dependent and independent variables that simplify Eq. (48) are $z \to \xi$ and $u(z) \to w(\xi)$, where[17]

$$\xi = \arctan \mathrm{e}^{-z} \,, \qquad w = \frac{u}{\sqrt{1+\mathrm{e}^{-2z}}} \,. \tag{49}$$

The infinite domain $-\infty < z < \infty$ corresponds to the finite domain $\pi/2 > \xi > 0$. The dependent variable $w(\xi)$ satisfies a second order ordinary differential equation with constant coefficients,

$$\frac{\mathrm{d}^2 w}{\mathrm{d}\xi^2} + (1 + 4\Lambda) w = 0 \,. \tag{50}$$

Two independent solutions of Eq. (50) are $\sin(\sqrt{M}\xi)$ and $\cos(\sqrt{M}\xi)$, where $M \equiv 1 + 4\Lambda$. Therefore, assuming $M \neq 0$, the general solution for $u(z)$ can be expressed as

$$u(z) = \sqrt{1+\mathrm{e}^{-2z}}\left[C_1 \sin\left(\sqrt{M}\arctan \mathrm{e}^{-z}\right) + C_2 \cos\left(\sqrt{M}\arctan \mathrm{e}^{-z}\right)\right] \,, \tag{51}$$

where C_1 and C_2 are constants. For $M = 0$ the solution is

$$u(z) = \sqrt{1+\mathrm{e}^{-2z}}\left[C_1 \arctan \mathrm{e}^{-z} + C_2\right] \,. \tag{52}$$

In the limit $z \to +\infty$ the solutions for $M \neq 0$ and $M = 0$ are bounded. However, in the limit $z \to -\infty$, the solutions may be unbounded. Boundedness of the solutions as $z \to -\infty$ requires the following necessary conditions on C_1 and C_2 be satisfied,

$$\begin{aligned} &C_1 \sin(\sqrt{M}\pi/2) + C_2 \cos(\sqrt{M}\pi/2) = 0 \,, && \text{for} \quad M \neq 0 \,, \\ &C_1\pi/2 + C_2 = 0 \,, && \text{for} \quad M = 0 \,. \end{aligned} \tag{53}$$

Substituting these relations in Eqs. (51) and (52) results in the following expressions for $u(z)$

$$u(z) = \sqrt{1+\mathrm{e}^{-2z}} \sin\left[\sqrt{M}\left(\frac{\pi}{2} - \arctan \mathrm{e}^{-z}\right)\right] \,, \quad \text{for} \quad M \neq 0 \,, \tag{54}$$

$$u(z) = \sqrt{1+\mathrm{e}^{-2z}}\left(\frac{\pi}{2} - \arctan \mathrm{e}^{-z}\right) \,, \quad \text{for} \quad M = 0 \,. \tag{55}$$

It turns out that the conditions (53) are also sufficient for the boundedness of $u(z)$. The limits of $u(z)$ as $z \to \pm\infty$ are

$$\begin{aligned} &u_- = \sqrt{M} \,, \quad u_+ = \sin\frac{\sqrt{M}\pi}{2} \,, && \text{for} \quad M \neq 0 \,, \\ &u_- = 1 \,, \quad u_+ = \frac{\pi}{2} \,, && \text{for} \quad M = 0 \,. \end{aligned} \tag{56}$$

From Eqs. (56), it is evident that no localized modes exist on the field lines with $y_0 = 0$. This is so because at the end $z \to -\infty$, where the field lines end up on the ridge instead of the flat side, the mode amplitude u_- never drops to zero independent of the value of Λ. The spectrum thus is purely continuous. Analogous to the case $x_0^2 = y_0^2$, the continuous spectrum includes the entire complex ω plane. Unstable continuum modes are therefore allowed.

A remnant, so to speak, of discrete modes is given by Eq. (54) with $\sqrt{M} = 2m$, $m = 1, 2, \cdots$, because, according to Eqs. (56), $u(z)$ still attains zero as $z \to +\infty$. In terms of Λ, this constraint on M implies $\Lambda = \Lambda_m$, where

$$\Lambda_m = m^2 - \frac{1}{4} \,, \tag{57}$$

which is close to the corresponding expression, Eq. (40), found for the field lines labeled $x_0^2 = y_0^2$. If $\Lambda = \Lambda_m$, the associated mode amplitude, Eq. (54), simplifies considerably. For example, the lowest two modes become

$$\begin{aligned} u_1(z) &= \frac{2}{(\mathrm{e}^{2z}+1)^{\frac{1}{2}}} \,, \\ u_2(z) &= -4\frac{\mathrm{e}^{2z}-1}{(\mathrm{e}^{2z}+1)^{\frac{3}{2}}} \,. \end{aligned} \tag{58}$$

The multiplicity of the continuous spectrum for $x_0^2 = y_0^2$ is lost in Eqs. (54)-(55), since the ratio of C_1/C_2 is now fixed.

Several stable continuum modes computed from Eq. (54) are shown in Fig. 5 for $\Lambda = 0.125$, 0.75 and 100. Among them, $\Lambda = 0.75$ corresponds to a "remnant" mode. Compared to the modes on the $x_0^2 = y_0^2$ field lines, shown in Fig. 3, the $y_0 = 0$ modes are much more pronounced towards the singular side $z < 0$.

For unstable modes, depicted in Fig. 6, the tendency to avoid the central region agrees with the behavior for $x_0^2 = y_0^2$ shown in Fig. 4. On the singular side, the mode amplitude tends to be smaller.

The equation governing the mode structure on the field line $x_0 = 0$, derived from Eq. (31), follows simply by replacing z in Eq. (48) with $(-z)$. All solutions for this case are therefore obtained by replacing z with $(-z)$ in the mode functions derived in this Section.

5c. Intermediate Magnetic Field Lines $0 < \alpha < 1$

So far we have explored the spectrum and the eigenfunctions on the field lines labeled $y_0^2/x_0^2 = 1$, $y_0^2/x_0^2 = 0$ and $y_0^2/x_0^2 = \infty$. Now we treat general values of $\alpha \equiv y_0^2/x_0^2$. This can only be done numerically. The essence of the results is a smooth transition from the behavior at the middle field lines towards the limiting field lines. Two techniques were used to solve the problem numerically. The first technique is based on a commercial eigenfunction and eigenvalue solver. A second technique that proved particularly useful is based on the standard shooting method to determine the value of the derivative du/dz at some position $z \ll -1$ that is required to produce a desired value of u at some position $z \gg 1$. A comparison of both methods and with analytic solutions produced excellent agreement.

Numerical results for the discrete spectrum and for localized modes for α in the region between zero and one are shown in Figs. 7 and 8. Note that in the region $1 \leq \alpha \leq \infty$, namely in the regions between the middle field lines and the polar field lines, the solutions of the mode equation can be obtained by a simple transformation from those of the region $0 \leq \alpha \leq 1$. This follows from Eq. (31) which remains unchanged if x_0^2 and y_0^2 are interchanged, i.e. if α is replaced by $1/\alpha$, and z is replaced by $-z$. This mirror symmetry corresponds to the mirror symmetry of the equilibrium configuration.

In Fig. 7, the lowest two eigenvalues Λ_m are displayed as functions of α. The dependence on α, in both cases, is slight, in particular for α of order one. It is monotonous only for Λ_1 but not for Λ_2. The limiting values for $\alpha \ll 1$ are close to 0.75 and 3.75, respectively. These are the eigenvalues of the lowest two remnant continuum modes, as discussed in connection with Eq. (57) above.

Figure 8 shows how the lowest discrete eigenfunction, $u_1(z)$, depends on α. The value of α decreases by a factor of 10 from curve to curve, from $\alpha = 1$ to $\alpha = 10^{-9}$. The rightmost curve corresponds to the analytic solution $u_1(z)$ from Eqs. (41). It is evident that the extension of $u(z)$ towards negative z increases logarithmically for decreasing $\alpha \ll 1$, while the extension on the side $z > 0$ stays more or less fixed. This tendency fits in nicely with the analytic results obtained above for $\alpha = 0$ since, with decreasing α, a flat region develops at $z < 0$ and grows in extent. In the limit $\alpha \to 0$ (which cannot be handled well by the numerical routine), the flat region becomes infinitely long, and no decay towards zero takes place anymore. Note that the normalization of the curves in Fig. 8 was chosen by the eigenfunction solving routine.

For continuum modes, at a fixed value of Λ, numerical experience indicates that an infinity of modes exists also for α in the region $0 < \alpha < 1$, just as for $\alpha = 1$. This is corroborated by Figs. 9 and 10. Both figures show a sequence of numerically obtained continuum modes $u(z)$, with an arbitrary value of $\Lambda = 1/\sqrt{3}$ held fixed. The sequence parameter α has the values $\alpha = 1$, 10^{-1}, 10^{-2} and 10^{-3}. In Fig. 9, the solution for $\alpha = 1$, which is the upper thick curve, coincides with the *symmetric* analytic solution, Eq. (42). In Fig. 10, the solution for $\alpha = 1$, which is the thick curve that passes through the origin, coincides with the *antisymmetric* analytic solution, Eq. (43). In both figures the modes $u(z)$ with decreasing α tend towards the *same* limit. This agrees with the analytic continuum mode for $\alpha = 0$ and $\Lambda = 1/\sqrt{3}$, Eq. (54) (second thick curve). Since sequences exist that originate from symmetric and from antisymmetric modes at $\alpha = 1$, it is plausible that sequences from intermediate modes exist as well. Figures 9 and 10 were obtained using the shooting method described in the first paragraph of this Section.

Recall that α can be interpreted as a "poloidal" coordinate on the magnetic surfaces (if z is viewed as a "toroidal" coordinate). Thus, the sequence of modes in Figs. 9 and 10 shows that for fixed frequency, i.e. fixed Λ, continuum modes exist that cover the magnetic surface smoothly. It is straightforward to also join the octants $0 \leq \alpha \leq 1$ and $1 \leq \alpha \leq \infty$ smoothly. It is a remark-

able result that the continuum Alfvén modes familiar from e.g. axisymmetric toroidal configurations[18] survive also in configurations without symmetry. In the toroidal model problem mentioned before, this result was also observed.[13,19] In Fig. 7 the frequency regions where any continuum mode can be smoothly extended to cover the entire magnetic surface are delimited by horizontal lines. It is inside the "empty" bands where such global continuum modes, as shown e.g. in Figs. 9 and 10, exist. In the bands around Λ_m, $m = 1, 2, \ldots$, however, a localized mode coexists with continuum modes at least along one field line (per octant).

Note that in the sequence of modes in Figs. 9 and 10 the boundary values u_- at $z \to -\infty$ need not be fixed for all field lines at the same constant value ($= 1$). Instead, the values of u_- may be chosen as an arbitrary periodic function of a poloidal angle (except for $\alpha = 0$ were u_- must be non-zero). This introduces one more degree of freedom for these global Alfvén modes.

6. Alfvén Continuum on Arbitrary Magnetic Surfaces

In this Section, we treat the spectral equation on field lines that lie outside the near region of the magnetic axis. If the field lines are not restricted to the vicinity of the axis, no exact analytic results can be obtained. Numerical solutions of the spectral equation are required in order obtain detailed information about the continuum.

Some general properties of the continuum can be found by considering the spectral equation at for $z \to \pm\infty$. In this limit, the field line equations can be approximated by (see Eqs. (17))

$$\frac{\mathrm{d}x}{\mathrm{d}z} = -\tan x \,, \qquad \frac{\mathrm{d}y}{\mathrm{d}z} = \mathrm{e}^{-2z} \sin y \,, \tag{59}$$

which can be integrated to give

$$\sin x = \sin x_1 \cdot \mathrm{e}^{-(z-z_1)} \,, \qquad \tan^2 \frac{y}{2} = \tan^2 \frac{y_1}{2} \cdot \exp\left(\mathrm{e}^{-2z_1} - \mathrm{e}^{-2z}\right) \,, \tag{60}$$

where the solution passes through the point (x_1, y_1, z_1), with $1 \ll z_1 \leq z$. It is evident from Eq. (60) that the x coordinate of the field line approaches zero asymptotically as e^{-z}, and y tends towards a constant value exponentially. This agrees with the near-axis case, Eqs. (30), with the exception that y^2 need not be small here. Using the exact equilibrium quantities, Eqs. (15)

and (17), the asymptotic forms of p and s for $x^2 \ll 1$ and $z \gg 1$, as derived from Eq. (22), are $p = x^2 e^{3z}$ and $s = 4x^2 e^z$, respectively. These expressions are independent of the potentially large asymptotic value of y^2, and also agree with the near-axis result given by Eqs. (29). Thus, as a function of the distance to the axis, the field line orbits and all other relevant equilibrium quantities remain asymptotically identical in the equilibrium end-regions on all magetic surfaces. Consequently, the general qualitative features of the continuum will be identical to those found in the region about the magnetic axis. In particular, the continuum consist of two components, a localized component at real frequencies, and a extended component at all complex frequencies. The extended component of the continuum can be unstable.

As mentioned previously, eigenvalues and eigenmodes can be found in principle by substituting into Eq. (21), the mode equation, the quadrature representations of $x(z)$ and $y(z)$ derived in Appendix A, and solving the resulting eigenvalue problem for $u(z)$ and Λ. For the present purposes, however, it is advantageous to solve numerically Eq. (19) for $x(z)$ and $y(z)$ and the mode equation for $u(z)$ without the use of the quadrature expressions. Using this purely numerical technique, we studied the effect of the distance to the axis on discrete and continuum modes. We treated only a few cases that illustrate the properties of the continuum modes away from the near-region of the magnetic axis. For example, only modes symmetric in z were considered.

In order to obtain the solution of Eq. (21) for the eigenmodes $u(z)$, the shooting method from some fixed initial point $z_- \ll -1$ to some fixed end point $z_+ \gg 1$ was applied in two steps. First only the field line equations given by Eq. (19) are considered. The initial values x_- and y_- for x and y, respectively, at $z = z_-$ have to be determined in such a way that the central values x_0 and y_0 are equal and assume a value within a desired range. In the second step of this process, the mode equation, Eq. (21), is solved together with the field line equations. The initial values x_- and y_- are now fixed, and the shooting parameter at $z = z_-$ is $\mathrm{d}u/\mathrm{d}z$. For discrete modes, Λ is an additional shooting parameter.

The result, for discrete modes with two nodes, is shown in Fig. 11. The thick curve is the analytic solution $u_3(z)$ from Eqs. (41) with $\Lambda = 9$. It corresponds to the limit $d_0 \to 0$, where the distance parameter d_0 is defined by $d_0 \equiv |x_0| = |y_0|$. The other two curves correspond to $d_0 = 0.5$ and 0.8, and the corresponding eigenvalues are $\Lambda = 7.85$ and 5.81, respectively. While the

amplitudes in the figure are arbitrary, it can still be seen that the eigenmodes get slightly narrower with increasing distance to the axis. The effect of d_0 on the eigenvalue, obviously, is rather strong.

The effect of d_0 on a stable continuum mode is shown in Fig. 12. Λ equals $1/\sqrt{3}$ throughout. Here, the thick curve is $u(z)$ from Eq. (42) as in Fig. 9. The other curves correspond to $d_0 = 0.3,\ 0.5$ and 0.8. The central peak of this mode increases with increasing distance to the axis, and it gets slightly broader. Analogously, for unstable continuum modes, the central depression, visible in Fig. 4, becomes slightly broader with increasing d_0.

All together, the effect of the distance to the axis is simply a quantitative one. Discrete and continuum modes persist at values of d_0 that are not small.

7. Summary and Conclusions

In this paper the shear Alfvén continuum in a spatially *asymmetric* plasma configuration has been explored. The equilibrium, which is an exact solution of the equations of ideal magnetohydrodynamics, is parallel to an infinite straight magnetic axis.[1] The lines of force of the equilibrium magnetic field form magnetic surfaces that close about this axis. For a low beta plasma, the Alfvén continuum mode is governed by a second order ordinary differential equation along the magnetic force lines. It is this case of a low beta plasma that has been explicitly treated.

On magnetic surfaces that neighbor the magnetic axis, the second order continuum equation reduces to a form that is solvable analytically along certain magnetic field lines. Using the analytic solutions, two general classes of solutions and therefore spectral components of the low beta mode equation have been identified: a localized component characterized by modes that decay to zero along magnetic field lines, and a non-localized component characterized by modes that approach non-zero constants at the plasma ends. The allowed frequencies of the localized modes are real and discrete, while the non-localized modes exist for all complex frequencies. Plots of the localized and non-localized mode functions were presented. For the non-localized mode, the numerical plots were restricted to purely real and imaginary frequencies. Non-localized modes in the continuous spectrum along a specific field line can be joined in general with those on neighboring field lines to form modes that

smoothly cover the entire magnetic surface. These extended continuum modes are the analogues of the Alfvén continuum modes that occur in the presence of either cylindrical, helical or axial symmetry. Numerical solutions of the Alfvén continuum equation on other field lines and on magnetic surfaces further from the magnetic axis confirm the results obtained with the analytic solutions.

Since the non-localized continuum modes exist for all complex frequencies, instability is implied if the frequency has a negative imaginary part. This instability, however, depends on boundary conditions specified at the ends of the infinite plasma configuration. It is not excited by forces internal to the plasma.

The localized modes, which in this study have been termed *nonsymmetry induced Alfvén eigenmodes* (NAE), are new. They do not occur in symmetric plasma configurations. It is conceivable that they play an important role in the interaction of the plasma with externally applied waves or fast particles.

Although this study is based on a particular asymmetric straight configuration, it is likely that the results have relevance for asymmetric toroidal plasmas.

Appendix A: Integration of field line equations

Equation (19) for the field line coordinates $x(z)$ and $y(z)$ can always be integrated up to quadratures if magnetic surfaces $F(x, y, z) = \text{const}$ are known, as is the case here. This can be seen as follows. An ansatz for the magnetic field $\mathbf{B}$ in the form

$$\mathbf{B} = [\nabla F(x, y, z) \times \nabla \hat{G}(x, y, z)] \tag{A.1}$$

is made. The intersection of the surfaces $F = \text{const}$ and $\hat{G} = \text{const}$ are field lines since $\mathbf{B} \cdot \nabla F = \mathbf{B} \cdot \nabla \hat{G} = 0$ implies embedding of $\mathbf{B}$ in both surfaces and the intersection of two surfaces is a line. The relation $F(x, y, z) = \text{const}$ can be inverted, to give $y = Y(F, x, z)$. This defines a function $G(F, x, z) \equiv \hat{G}(x, Y(F, x, z), z)$ which allows the new representation

$$\mathbf{B} = [\nabla F(x, y, z) \times \nabla G(F, x, z)] \; . \tag{A.2}$$

Again, $\mathbf{B} \cdot \nabla G = 0$, so that $G = \text{const}$ at $F = \text{const}$ also describes magnetic field lines. Once G is determined, however, $G(F, x, z) = const$ is a (in general

implicit) representation of the solution $x = x(z)$. Analogously, with a function $H(F, y, z)$ the solution for $y = y(z)$ can be found.

From Eq. (A.2) one obtains

$$\partial_x G = \frac{-B_z}{\partial_y F} , \qquad \partial_z G = \frac{B_x}{\partial_y F} , \tag{A.3}$$

where $\partial_x = \partial/\partial x$, etc. The y component of Eq. (A.2) is equivalent to $\mathbf{B} \cdot \nabla F = 0$ and thus is trivially satisfied. From Eqs. (A.3) a compatibility condition results,

$$\partial^2_{xz} G = \partial^2_{zx} G . \tag{A.4}$$

Using $\partial_y(\mathbf{B} \cdot \nabla F) = 0$ and $\nabla \cdot \mathbf{B} = 0$, it can be shown that Eq. (A.4) is automatically satisfied. Consequently, Eqs. (A.3) can be integrated, with the result

$$G(F, x, z) = -\int_{x_0}^{x} \mathrm{d}\tilde{x} \, \frac{B_z}{\partial_y F}(F, \tilde{x}, z) + \int_{z_0}^{z} \mathrm{d}\tilde{z} \, \frac{B_x}{\partial_y F}(F, x_0, \tilde{z}) , \tag{A.5}$$

where x_0 and z_0 are arbitrary integration constants. If the field line $G = G_0 = \text{const}$ is supposed to pass through the point $x = x_0$ and $z = z_0$ the constant G_0 is zero. Equation (A.5), with $G = 0$, represents an implicit form of the promised coordinate function $x = x(z)$. Analogously, $y = y(z)$ is obtained. In general, and in particular for the present functions $\mathbf{B}(x, y, z)$ and $F(x, y, z)$, the quadratures involved cannot be resolved analytically.

Appendix B: Self-adjointness and boundary conditions

Let the operator $\mathcal{L}$ be

$$\mathcal{L} \equiv \frac{-1}{s(z)} \frac{\mathrm{d}}{\mathrm{d}z} \left[p(z) \frac{\mathrm{d}}{\mathrm{d}z} \right] , \tag{B.1}$$

with real coefficients $s(z)$ and $p(z)$. Equation (21) then takes on the form

$$\mathcal{L}u = \Lambda u . \tag{B.2}$$

Multiplication of Eq. (B.2) with $s(z)$ and a solution $v(z)$, and integration from $-a$ to $+a$ gives, after two partial integrations,

$$(v, \mathcal{L}u) = \left(pv \frac{\mathrm{d}u}{\mathrm{d}z} - pu \frac{\mathrm{d}v}{\mathrm{d}z} \right) \Bigg|_{-a}^{+a} + (u, \mathcal{L}v) , \tag{B.3}$$

where

$$(f,g) \equiv \int_{-a}^{+a} sf\mathcal{L}g \, \mathrm{d}z \ , \tag{B.4}$$

and $a \to \infty$ is intended. The operator $\mathcal{L}$ is self-adjoint, provided the quantity S vanishes,

$$S(v,u) \equiv \left(pv\frac{\mathrm{d}u}{\mathrm{d}z} - pu\frac{\mathrm{d}v}{\mathrm{d}z} \right) \Bigg|_{-\infty}^{+\infty} = R(v,u) - R(u,v) = 0 \ . \tag{B.5}$$

Taking for u the most general solution, and $v = u^*$, this condition implies

$$S(u^*,u) = R(u^*,u) - R(u,u^*) = 2i\,\Im\, R(u^*,u) = 0 \ , \tag{B.6}$$

i.e. the imaginary part of $R(u^*,u)$ has to vanish. From Eq. (44), with complex Λ, and $R = \Re R + i\,\Im R$, it follows that $S = 0$ is equivalent to $\Im\,\Lambda = 0$. This conclusion – that Λ should be real – is valid, provided R is bounded. For $x_0^2 = y_0^2$, R can be evaluated and is found to be bounded without any restrictions on the boundary values of u.

For $y_0 = 0$, this is not the case in general. For $M = 1+4\Lambda > 0$, for example, R diverges proportional to e^a, for $a \to \infty$, as an analysis with Eqs. (48) and (51) reveals. The divergence originates at the end $z \to -\infty$. It is only avoided if $u(z \to -\infty)$ stays bounded, or, equivalently, if $\mathrm{d}u/\mathrm{d}z = 0$ there. With these boundary conditions the conclusion that Λ be real is recovered.

Note that the boundary conditions just mentioned are identically satisfied not only if $x_0^2 = y_0^2$ but also if x_0 and y_0 are not zero.

References

[1]R. Kaiser and A. Salat, Phys. Rev. Lett. **77**, 3133 (1996).

[2]Preliminary results of the present study were first reported in the following references: A. Salat and J. A. Tataronis, Bull. Am. Phys. Soc. **41**, 1612 (1996); A. Salat and J. A. Tataronis, *Proceedings of the 1997 International Sherwood Fusion Theory Conference, Madison, 1997* (University of Wisconsin, Madison, 1997), p. 2C02; A. Salat and J. A. Tataronis, *Proceedings of the 24th European Physical Society Conference on Controlled Fusion and Plasma Physics, Berchtesgaden, 1997*, "The shear Alfvén continuum of an ideal MHD equilibrium without spatial symmetry", to be published.

[3]H. Grad, Phys. Fluids **10**, 137 (1967).

[4]J. P. Freidberg, *Ideal Magnetohydrodynamics*, (Plenum Press, New York, NY, 1987), p. 240.

[5]J. A. Tataronis, J. N. Talmadge, and J. L. Shohet, Comments Plasma Phys. Controlled Fusion **7**, 29 (1982).

[6]M. P. Bernardin and J. A. Tataronis, Phys. Fluids **27**, 133 (1984).

[7]G. O. Spies, Nucl. Fusion **19**, 1532 (1979).

[8]E. Hameiri, Commun. Pure Appl. Math. **Vol. XXXVIII**, 43 (1985).

[9]C. Z. Cheng, L. Chen, and M. S. Chance, Ann. Phys. (NY) **161**, 21 (1985), C. Z. Cheng and M. S. Chance, Phys. Fluids **29**, 3695 (1986).

[10]R. Kaiser and A. Salat, J. Plasma Phys. **57**, 425 (1997).

[11]J.P. Freidberg, H. Weitzner, and D. Weldon, Plasma Phys. **12**, 987 (1970).

[12]V. A .Yakubovich and V. M. Starzhinskii, *Linear Differential Equations with Periodic Coefficients*, (Wiley, New York, NY, 1975), Vol. 1.

[13]A. Salat, Plasma Phys. Contr. Fusion **34**, 1339 (1992).

[14]B. Simon, Advances Appl. Math. **3**, 463 (1982).

[15]Z. Yoshida, Phys. Rev. Lett. **68**, 3168 (1992), Y. Yamakoshi, K. Muto, and Z. Yoshida, Phys. Rev. E **50**, 1437 (1994).

[16]I. B. Bernstein, E. A. Frieman, M. D. Kruskal, and R. M. Kulsrud, Proc. Roy. Soc. A, **244**, 17 (1958).

[17]A. D. Polyanin and V. F. Zaitsev, *Handbook of Exact Solutions for Ordinary Differential Equations*, (CRC Press, Boca Raton, CA, 1995).

[18]J. P. Goedbloed, Phys. Fluids **18**, 1258 (1975), Y. Pao, Nucl. Fusion **15**, 631 (1975).

[19]A. Salat, Z. Naturforsch. **37a**, 830 (1982).

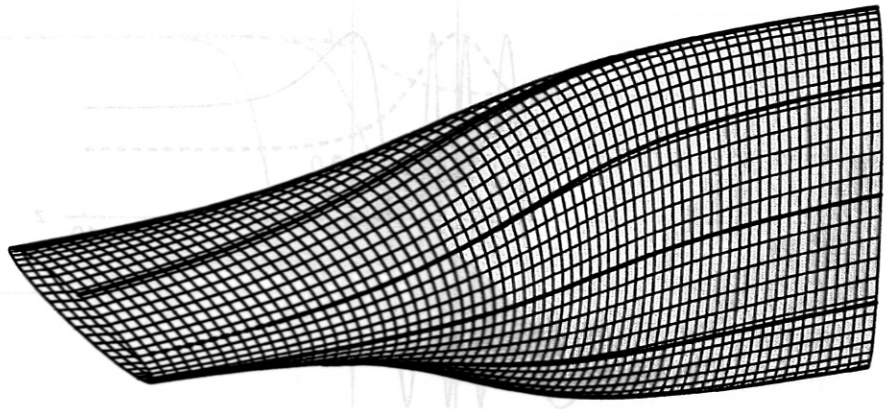

Figure 1: Magnetic surface $F = 1.0$. With four field lines (thick).

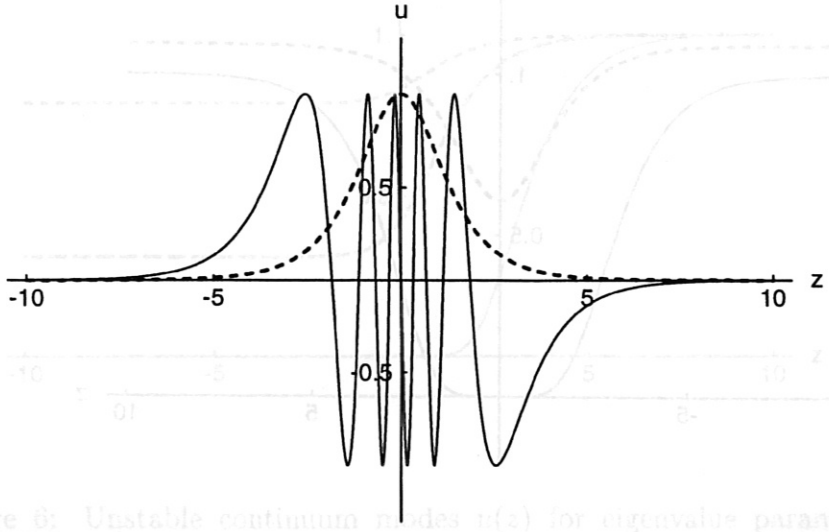

Figure 2: Eigenfunctions $u_1(z)$ (dashed) and $u_{10}(z)$ (solid). For $x_0^2 = y_0^2$.

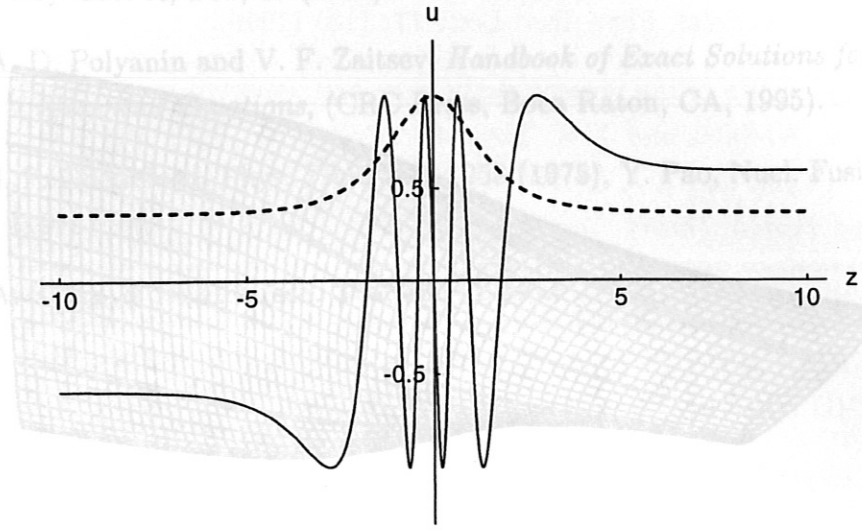

Figure 3: Stable continuum modes $u(z)$ for eigenvalue parameter $\Lambda = 1/\sqrt{3}$ (dashed) and $\Lambda = 100/\sqrt{3}$ (solid). For $x_0^2 = y_0^2$.

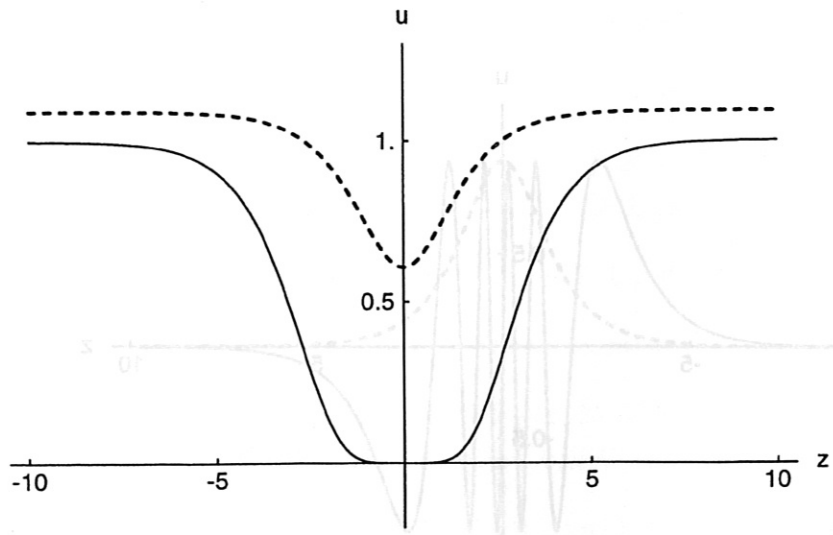

Figure 4: Unstable continuum modes $u(z)$ for eigenvalue parameter $\Lambda = -1/\sqrt{3}$ (dashed) and $\Lambda = -100/\sqrt{3}$ (solid). For $x_0^2 = y_0^2$.

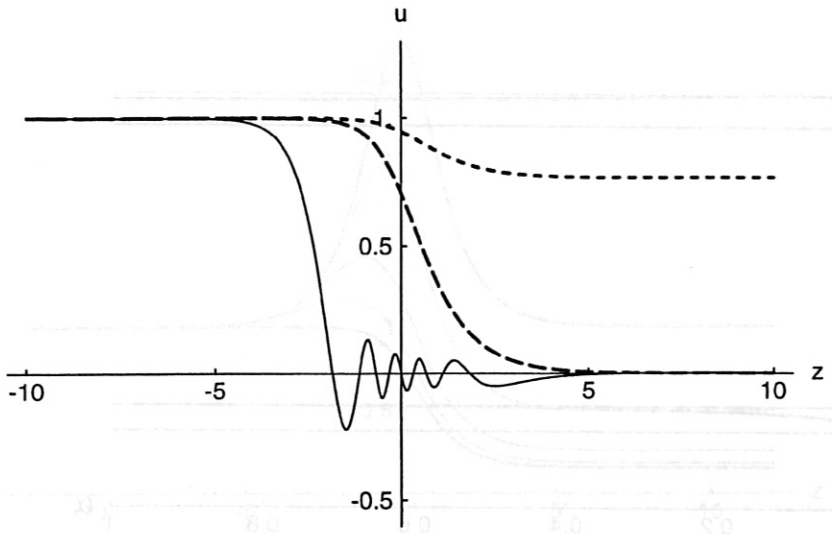

Figure 5: Stable continuum modes $u(z)$ for eigenvalue parameter $\Lambda = 0.125$ (short dashed), $\Lambda = 0.75$ (long dashed) and $\Lambda = 100$ (solid). For $y_0 = 0$.

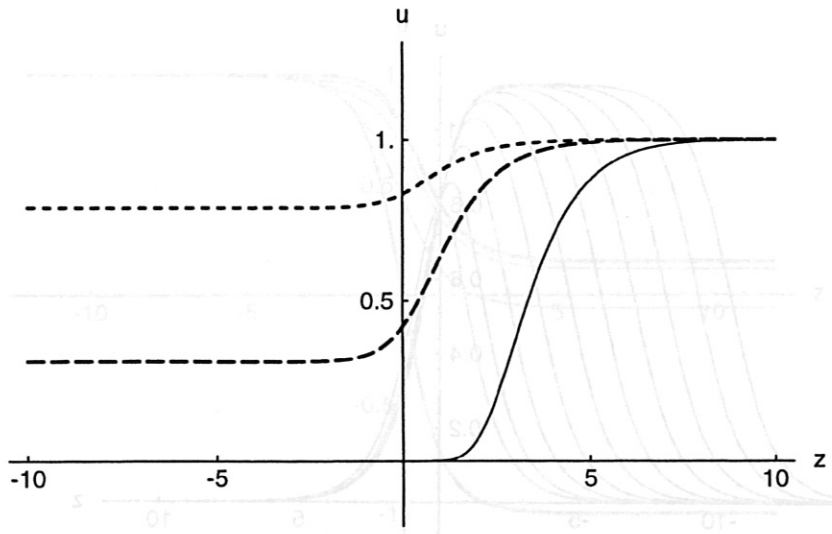

Figure 6: Unstable continuum modes $u(z)$ for eigenvalue parameter $\Lambda = -0.125$ (short dashed), $\Lambda = -0.75$ (long dashed) and $\Lambda = -100$ (solid). For $y_0 = 0$.

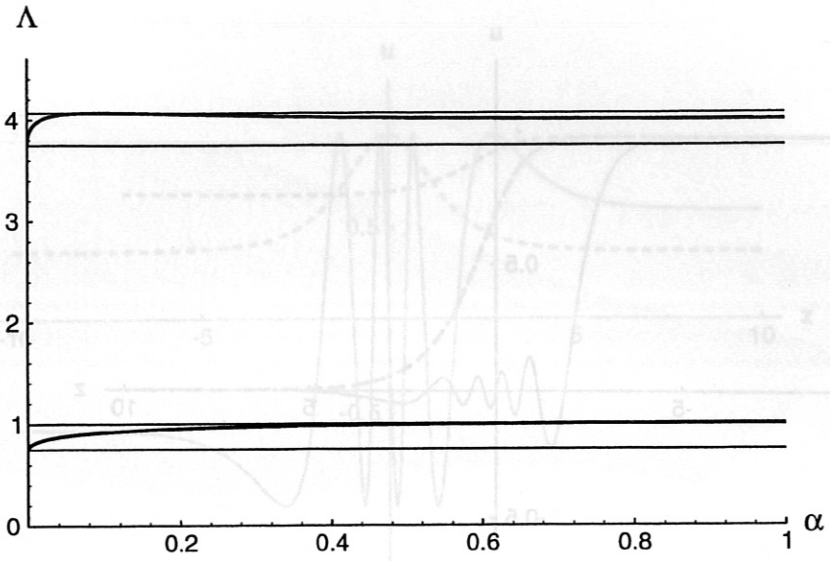

Figure 7: Dependence of eigenvalue Λ_1 (lower curve) and Λ_2 (upper curve) on field line position $\alpha = y_0^2/x_0^2$. Horizontal lines delimit regions with or without localized modes.

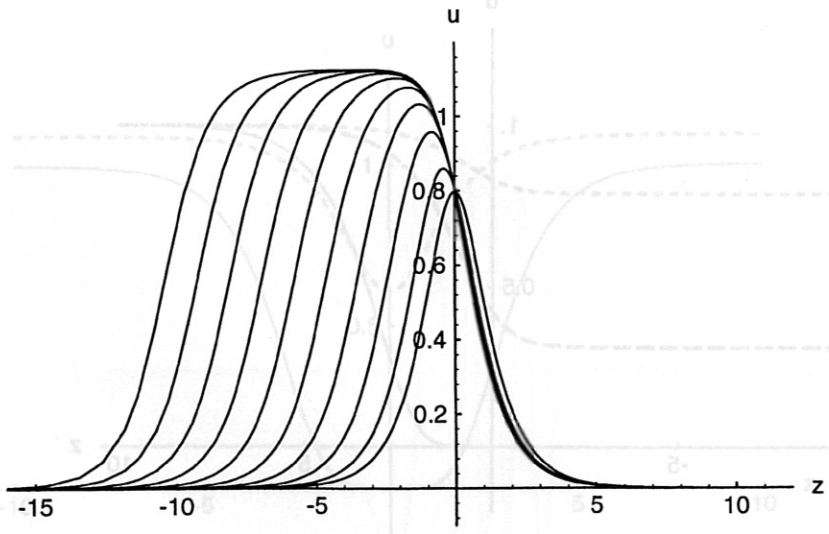

Figure 8: Dependence of eigenmode $u_1(z)$ on field line position α. Rightmost curve: $\alpha = 1$. Curves to the left: α decreases by a factor of 10 from curve to curve.

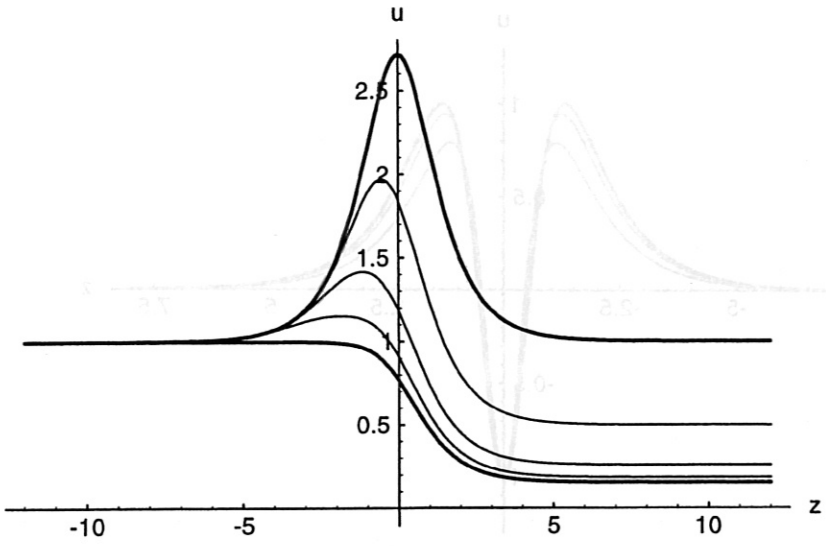

Figure 9: Dependence of continuum modes $u(z)$ on field line position α: $\alpha = 1$ (*symmetric* solution, thick curve), $\alpha = 10^{-1},\ 10^{-2},\ 10^{-3}$ (curves in descending order) and $\alpha = 0$ (lower thick curve). With $\Lambda = 1/\sqrt{3}$ fixed.

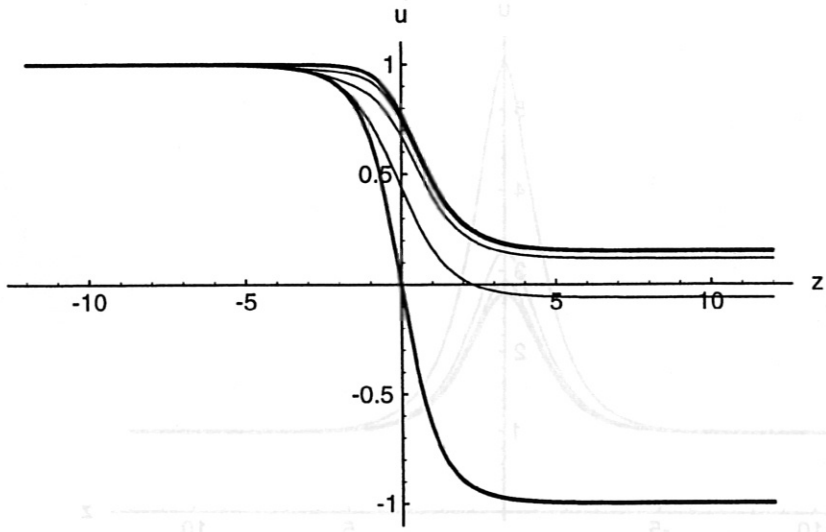

Figure 10: Dependence of continuum modes $u(z)$ on field line position α: $\alpha = 1$ (*antisymmetric* solution, thick curve), $\alpha = 10^{-1},\ 10^{-2},\ 10^{-3}$ (curves in ascending order) and $y_0 = 0$ (second thick curve). With $\Lambda = 1/\sqrt{3}$ fixed.

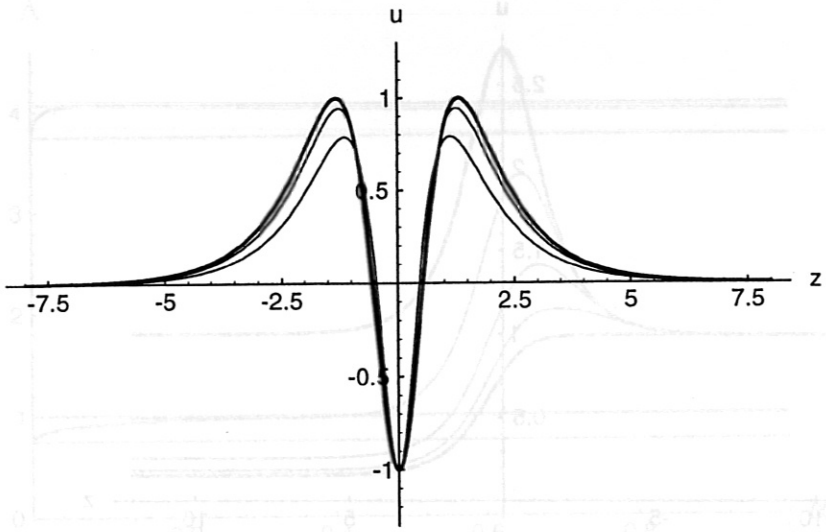

Figure 11: Dependence of localized symmetric eigenmode $u_3(z)$ on distance to the axis. Distance parameter $d_0 \ll 1$ (thick curve), $d_0 = 0.5$ (middle curve), and $d_0 = 0.8$ (lower curve). For $x_0^2 = y_0^2$.

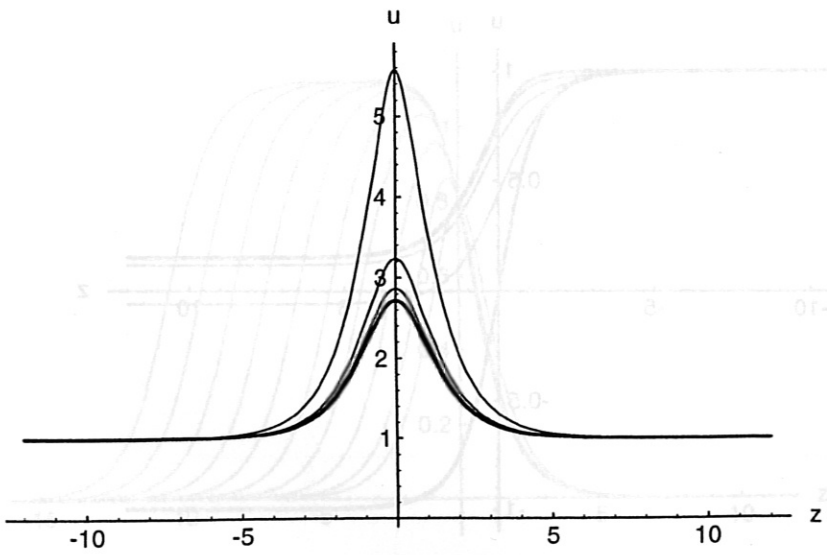

Figure 12: Dependence of symmetric continuum mode $u(z)$, with eigenvalue parameter $\Lambda_0 = 1/\sqrt{3}$, on distance to the axis. $d_0 \ll 1$ (thick curve), $d_0 = 0.3,\ 0.5$ and 0.8 (largest amplitude). For $x_0^2 = y_0^2$.